SSC-218

The Superconducting Super Collider

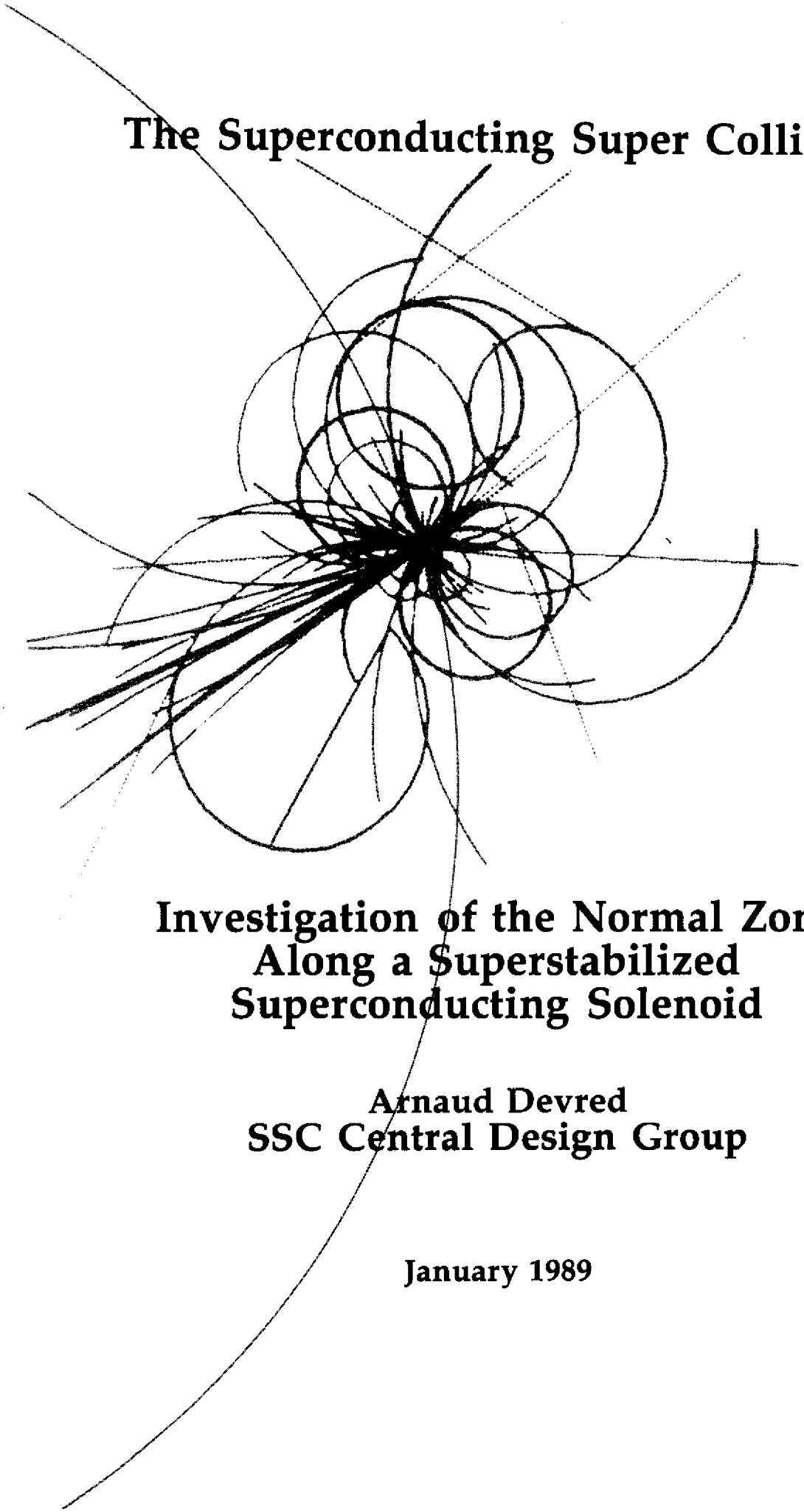

Investigation of the Normal Zone Along a Superstabilized Superconducting Solenoid

Arnaud Devred
SSC Central Design Group

January 1989

SSC-218

INVESTIGATION OF THE NORMAL ZONE ALONG A SUPERSTABILIZED SUPERCONDUCTING SOLENOID*

Arnaud Devred
SSC Central Design Group†
c/o Lawrence Berkeley Laboratory, Berkeley, California 94720

January 1989

"A la fin tu es las de ce monde ancien"
G. Appolinaire
Zone

* Submitted for publication to the Journal of Applied Physics.

† Operated by Universities Research Association, Inc., for the United States Department of Energy.

I. Introduction

In composite, multifilament conventional superconductors, normal zone propagation is a strictly thermal phenomenon. It occurs close to the transition front, where a fraction of the power dissipated in the normal zone is transmitted by conduction to the superconducting zone, which, in turn, heats up and goes into transition. In the simple model featuring a straight composite conductor with infinite length and axis (Oz) that is thermally insulated from the surrounding medium, with specific heat C and thermal conductivity k independent from temperature, it was determined long ago[1,2] that, if the current-sharing zone can be ignored, the temperature profile undergoes a constant-velocity asymptotic shift.

The propagation velocity v is given by

$$v = \left(\frac{D_{\text{th}} P_j}{\Delta H}\right)^{1/2} \quad , \tag{1}$$

where

$D_{\text{th}} = k/C$ is the equivalent thermal diffusivity ($m^2 s^{-1}$),

ΔH is the enthalpy per unit volume of the superconducting zone ($J\ m^{-3}$),

P_j is the average density (per unit volume) of the power dissipated in the normal zone ($W\ m^{-3}$).

(All the above are averaged over the conductor cross-section.)

It has also been shown that a time delay given by

$$\tau_p = \frac{D_{\text{th}}}{v^2} \tag{2}$$

is characteristic of the variations in the temperature profile when shifting.

In superstabilized conductors, like that developed for the ALEPH solenoid,[3] where a conventional composite is enclosed in a large section of aluminum, an electromagnetic diffusion phenomenon is added. Indeed, close to the transition front, the current previously carried by the filaments is expelled toward the copper, then toward the aluminum. But, given the large cross section of the aluminum, the current needs a certain amount of time and

space to diffuse itself into the aluminum. The transition front carries with it a wake of electromagnetic diffusion, along which the Joule power density per unit volume progressively decreases. In a previous paper[4] we examined the straight infinite conductor model and introduced variations in the power density per unit volume. If we postulate the existence of a constant-velocity asymptotic shift of the temperature profile T and of the magnetic induction B, supposing that such a shift was established beginning with $t = -\infty$ as z increases, the velocity v is given by

$$v\,\Delta H = \int_{-\infty}^{0} du\; P_j(u) + \int_{0}^{+\infty} du\; \exp\left(\frac{-uv}{D_{\mathrm{th}}}\right) P_j(u) \quad , \tag{3}$$

where

$u = vt - z$ is the length of the conductor, so that the superconducting zone fills the half-space $u \leq 0$ and the normal zone the half-space $u \geq 0$,

$\int_{-\infty}^{0} du\, P_j(u)$ is the integral of the density (per unit volume) of the power dissipated along the superconducting zone (which is not nil, as we anticipate diffusion close to the transition front), and

$\int_{0}^{+\infty} du\, \exp(-uv/D_{\mathrm{th}})$ is the Laplace transformation of the density (per unit volume) of the power dissipated in the normal zone, expressed in v/D_{th}.

(The above are all averaged over the conductor cross section.)

In addition, we have shown[5] that a characteristic time for the decrease of the power density per unit volume is given by

$$\tau_{\mathrm{m}} = \frac{L_2^2}{2D_m} \quad , \tag{4}$$

where L_2 and D_m are respectively the width and the electromagnetic diffusivity of the superstabilizer.

Equation (3) provides coupling of the thermal propagation and electromagnetic diffusion phenomena. The last quantity to be determined is thus $P_j(u)$.

In an actual solenoid, the electromagnetic behavior of a conductor cannot be dissociated from that of its neighbors. In this paper we consider the layer of straight, infinite conductors in Fig. 1a, which is representative of the ALEPH solenoid. From the thermal standpoint, only the axial propagation (along Oz) is relevant; we therefore disregard transverse propagation (perpendicular to Oz), assuming that the normal zone progresses simultaneously and identically along all the conductors. It follows that Eq. (3), although derived from a single conductor, remains valid. In view of the highly complex geometrical configuration of Fig. 1a (where the composite material does not fill the full width of the conductor, and conductors are separated by insulating material), calculations of electromagnetic phenomena are based on the set of infinite plates shown in Fig. 1b. Although these two configurations are different, and cannot be directly related, it is shown in the Appendix how the results for the infinite-plate model can be generalized to a rectangular geometry.

NOTE: In configuration 1b, average values are computed based on plate thickness ($2L_t$).

Until now, electromagnetic diffusion has only been investigated in the copper part of the composite, and from the standpoint of cryogenic stability.[6,7] Some measurements of the velocity have been made, but for a superstabilized conductor immersed in liquid helium.[8] A quench development analysis in a 1-m bore test coil is presented in Reference 9, but in such a configuration, the transverse propagation from turn to turn predominates. This work is part of the study we have made of the longitudinal propagation of the normal zone through indirectly cooled superconducting solenoids.[10] A general review of our results is given in Reference 11.

II. The Infinite-Plate Model

1. Geometrical considerations

In the geometrical configuration of Fig. 1b, the field lines are straight lines parallel to the Oz axis; we thus have $J_x(y,u) = 0$ for all y and all u. The Maxwell-Ampere equation for the quasi-stationary states then shows that the only relevant components are the (Ox) component of magnetic flux density and the (Oy) and (Oz) components of current density. Let subscripts 1 and 2 respectively, refer to the composite and the superstabilizer. These three components are identified as $B_i(y,u)$, $J_{yi}(y,u)$, and $J_{zi}(y,u)$, with $i = 1$ or 2.

We also assume that, throughout the duration of the phenomenon, the solenoid remains energized with constant current I. The average value of $J_{zi}(y,u)$ over plate thickness $2L_3$ is called J_0, and we write $B_0 = -\mu_0 J_0 L_3$. Conservation of current density shows that J_0 and B_0 are constants.

Last, in view of the fact that the plate model is extrapolated from a large solenoid, a distinction is made between the $y > L_3$ half-space outside the solenoid, where flux density is nil, and the inside half-space $y < -L_3$, where flux density is $2B_0$. Symmetry with respect to y is achieved by superimposing a uniform, constant flux density equal to B_0 (in this case, symmetry is odd with respect to B, and even with respect to J); the current distribution, the only quantity of interest, remains unchanged. In the following, investigations consider the $y \geq 0$ half-space.

2. Laws governing composite behavior

We assume that the composite behaves as a homogeneous, isotropic medium in which (1) Magnetic flux density $\breve{B}_1(y,u)$ at any point is linked to the magnetic field $\breve{H}_1(y,u)$ by the relationship $\breve{B}_1(y,u) = \mu_0 \breve{H}_1(y,u)$; for $0 \leq y \leq L_1$ and for all u. This assumption is equivalent to regarding the superconducting filaments as strongly penetrated. (2) The electric field $\vec{E}_1(y,u)$ is nil at all points in the superconducting zone. (3) Current density is uniform throughout all cross-sections of the normal zone, while resistivity ρ_1 of the composite in the

normal state is equal to the equivalent axial resistivity. This is equivalent to assuming that diffusion through the copper in the composite is instantaneous when measured on the same scale as diffusion through the superstabilizer. In a previous publication,[5] we have introduced the dimensionless parameter $m = \rho_2 L_1 / \rho_1 L_2$ where ρ_2 is the resistivity of the superstabilizer, and we have shown the above assumption to be justified as long as

$$m^2 \ll 1 \tag{5}$$

holds. Equation (5) defines a superstabilization criterion, and m is called the first superstabilization parameter.

3. Diffusion equations and boundary conditions

No heat is dissipated when the composite is in the super-conducting state; it is therefore not necessary to determine the magnetic induction profile.

When the composite is in the normal state, $J_{z1}(u)$ is assumed to be uniform through each section, and $B_1(y,u)$ to vary linearly with respect to y. Because of the odd symmetry and the conservation of the magnetic flux density normal component at $y = L_1$, we have

$$B_1(y,u) = B_2(y = L_1,u)\,\frac{y}{L_1} \qquad \text{for } 0 \le y \le L_1,\ u \ge 0 \quad .$$

In the superstabilizer, $B_2(y,u)$ is the solution of the magnetic diffusion equation

$$\left\{ \begin{array}{c} \dfrac{\partial^2 B_2(y,u)}{\partial y^2} + \dfrac{\partial^2 B_2(y,u)}{\partial u^2} = \dfrac{v}{D_m}\,\dfrac{\partial B_2(y,u)}{\partial u} \quad , \\ \text{for } L_1 \le y \le L_3, \text{ all } u \end{array} \right. \tag{6}$$

where $D_m = \rho_2 / \mu_0$ is the superstabilizer diffusivity.

Boundary conditions are

- **At $y = L_3$:**

$$B_2(y = L_3,u) = B_0 \qquad \text{for all } u \tag{7}$$

and

$$\beta_k = \left(k - \tfrac{1}{2}\right)\pi \quad .$$

Once (P_n) and (P_s) have been solved, a solution to problem (P) can be derived by fitting analytically $f(y,u)$ and $g(y,u)$ at $u = 0$, i.e., by determinating a set of coefficients $(a_k)_{k\in N^*}$ and $(b_k)_{k\in N^*}$ such that

$$\begin{cases} f(y,u=0) = g(y,u=0) \\ \dfrac{\partial f(y,u=0)}{\partial y} = \dfrac{\partial g(y,u=0)}{\partial y} \\ \text{for } L_1 \le y \le L_3 \end{cases} \quad .$$

Let us replace f and g by their expression and consider $l \in N^*$. The above equations can be mutiplied by $\sin[\beta_l (L_3 - y)/L_2)]$ and integrated between $y = L_1$ and $y = L_3$, eliminating b_l. A similar procedure can be followed by multiplying the two equations by $\sin[\alpha_l (L_3 - y)/L_2)]$ and eliminating a_l. This yields

$$\sum_{k=1}^{+\infty} a_k \frac{1 + (\lambda_k/\mu_l)}{\alpha_k^2 - \beta_l^2} = \frac{1}{(1+m)\beta_l^2} \qquad \text{for } l \in N^* \qquad (12)$$

$$\sum_{k=1}^{+\infty} b_k \frac{1 + (\mu_k/\lambda_l)}{\beta_l^2 - \alpha_k^2} = \frac{1}{\alpha_l^2} \qquad \text{for } l \in N^* \qquad (13)$$

Conditions (12) and (13) indicate a summation over the entire $k \in N^*$ range; they should be written for the entire $l \in N^*$ range. Let us now consider $N \in N^*$, and write conditions (14) and (15) derived from (12) and (13), retaining only those subscripts with values not exceeding N:

$$\sum_{k=1}^{N} a_k \frac{1 + (\lambda_k/\mu_l)}{\alpha_k^2 - \beta_l^2} = \frac{1}{(1+m)\,\beta_l^2} \qquad \text{for } 1 \le l \le N \qquad (14)$$

$$\sum_{k=1}^{N} b_k \frac{1 + (\mu_k/\lambda_l)}{\beta_l^2 - \alpha_k^2} = \frac{1}{\alpha_l^2} \qquad \text{for } 1 \le l \le N \quad . \qquad (15)$$

Conditions (14) and (15) reduce to linear systems with constant coefficients including N equations with N unknowns, which can be solved by numerical methods. Designating system solutions by $(a_k^N)_{k\varepsilon N}$ and $(b_k^N)_{k\varepsilon N}$, we write

$$f^N(y,u) = B_0\left[1 - \frac{L_3 - y}{(1+m)L_2} + \sum_{k=1}^{N} a_k^N f_k(y,u)\right]$$

and

$$g^N(y,u) = B_0\left[1 + \sum_{k=1}^{N} b_k^N g_k(y,u)\right] \quad .$$

At this stage, it can be verified both numerically and by changing the parameters in the problem equations that $f^N(y,u)$ and $g^N(y,u)$ converge toward a limit for large values of N, and that the limit encompasses the very solution derived for (P) through the DELPHINE program. It can therefore be stated that

$$\begin{cases} \lim\limits_{N\to+\infty} f^N(y,u) = B_2(y,u) & \text{for } (y,u) \in \Omega_n \\ \lim\limits_{N\to+\infty} g^N(y,u) = B_2(y,u) & \text{for } (y,u) \in \Omega_n \end{cases} \quad .$$

An approximate solution for (P) can thus be derived by solving Eqs. (14) and (15) for large values of N.

The quality of the fit at $u = 0$ provides some idea of the accuracy of the solution for (P). We write

$$r^N(y) = \frac{g^N(y,u=0) - f^N(y,u=0)}{f^N(y,u=0)} \quad .$$

As regards the numerical data of Tables I and II, we have verified that for values of y that are not close to L_1, the ratio $r^N(y)$ rapidly becomes negligible: N is of the order of 100 (Fig. 2a). However, as might be expected, convergence is much slower for values of y close to L_1 (Fig. 2b); it is precisely at point $(y = L_1, u = 0)$ that the condition changes form. This is

not a matter for concern, since the computation of P_J involves averaging over y and the divergence will be partly cancelled out.

5. Heating power profile

Except in the composite when in the superconducting state (where the electric field is nil), the electric field $\vec{E}$ is related to current density $\vec{J}$ through Ohm's law. The average power density per unit volume is then given by

$$P_J(u) = \frac{1}{L_t}\left\{ Y(u) \int_0^{L_1} dy\, \rho_1 \left[J_{1y}^2(y,u) + J_{1z}^2(y,u)\right] + \int_{L_1}^{L_2} dy\, \rho_2 \left[J_{2y}^2(y,u) + J_{2z}^2(y,u)\right]\right\} \quad ,$$

where $Y(u)$ is the Heaviside step function.

The components of current density are given by the Maxwell-Ampere equation for the quasi-stationary states. They are obtained by differentiating, term-by-term, the series used for computing $B_i\,(y,u)$.

An approximate expression for $P_j(u)$ is thus given by the following:

In the normal zone:

$$P_J(u) = P_{J0}\left\{ \frac{m}{1+m} + \frac{(mL_1)^2}{3} \sum_{k=1}^{N} \sum_{l=1}^{N} a_k^N\, a_l^N\, \lambda_k\, \lambda_l \exp\left[-(\lambda_k + \lambda_l)u\right] + \ldots \right.$$
$$\left. \ldots + \frac{m}{2} \sum_{k=1}^{N} (a_k^N)^2 \left[1 + \left(\frac{\lambda_k L_2}{\alpha_k}\right)^2\right] \left[1 + m + (m\alpha_k)^2\right] \exp(-2\lambda_k u)\right\} \quad . \tag{16}$$

In the superconducting zone:

$$P_J(u) = P_{J0}\, \frac{m}{2} \sum_{k=1}^{N} (b_k^N)^2 \left[\beta_k^2 + (\mu_k L_2)^2\right] \exp\,(2\mu_k u) \quad , \tag{17}$$

in which we use

$$P_{j0} = \frac{\rho_1}{L_t\, L_1} \left(\frac{B_0}{\mu_0}\right)^2 \quad .$$

(P_{j0} is the average density of the dissipated power, computed with the assumption that the current remains confined to the composite).

6. Implicit equation for propagation velocity

The approximate expression of $P_j(u)$ derived above can be introduced in Eq. (3). The final outcome of the calculation is

$$\frac{v\Delta H}{P_{j0}} = \frac{m}{1+m}\frac{D_{\text{th}}}{v} + \frac{(mL_1)^2}{3}\sum_{k=1}^{N}\sum_{l=1}^{N} a_k^N a_l^N \frac{\lambda_k\lambda_l}{(v/D_{\text{th}}) + \lambda_k + \lambda_l} + \tag{18}$$

$$+ \frac{m}{2}\sum_{k=1}^{N} (a_k^N)^2 \left[1 + m + (m\alpha_k)^2\right] \frac{1+\left(\frac{\lambda_k L_2}{\alpha_k}\right)^2}{(v/D_{\text{th}}) + 2\lambda_k} + \frac{m}{4}\sum_{k=1}^{N} \frac{(b_k^N)^2\left[\beta_k^2 + (\mu_k L_2)^2\right]}{\mu_k} .$$

Equation (18) can be solved numerically, thus providing an approximate value of the propagation velocity.

In Fig. 3, we have verified convergence by plotting v against N for the numerical data of Tables I and II. As mentioned earlier, the averaging introduced by Eq. (3) partly eliminates the irregularity at the point ($y = L_1$, $u = 0$).

The handling of Eq. (18) and linear systems (14) and (15) is rather cumbersome; while the results are satisfactory, little is learned about the physics of the phenomenon. To progress in that direction, and to derive an approximate form of Eq. (18), we will now investigate the two limiting cases $v \to 0$ and $v \to \infty$ (this variation of parameter v is physically achieved by changing the value of the current I).

III. Investigation of the Low-Velocity Domain

When v tends toward zero, the characteristic time τ_p of the thermal propagation phenomenon defined by Eq. (2) tends toward infinity, whereas the characteristic time τ_m of

the electromagnetic diffusion phenomenon, derived in Eq. (4), remains constant. At low velocities, it thus appears that

$$\tau_m \ll \tau_p \quad . \tag{19}$$

Relationship (19) can be interpreted as a scale discrepancy between the two phenomena. Thus, to an observer looking at the electromagnetic diffusion wake, the temperature profile appears to be strongly expanded. Conversely, an observer looking at the temperature profile would see the motion of the electromagnetic diffusion wake as fast and sudden. It could even be said that the second observer regards diffusion in the superstabilizer as instantaneous and views the average power density profile as a step function

$$P_j(u) = Y(u)\, P_{jss} \quad ,$$

where

$$P_{jss} = \frac{m}{1+m} P_{j0} \quad .$$

(P_{jss} is the limit of Eq. (16) when u tends toward $+\infty$. It is therefore the calculated power density, based on the assumption that the current is distributed between the composite and the superstabilizer, current densities being uniform.)

In short, the low-velocity domain exhibits an expansion of the temperature profile that conceals the electromagnetic wake.

The boundary of the low-velocity domain can be derived from Relationship (19). We have

$$v \ll \frac{D_e}{L_2} \quad , \tag{20}$$

where $D_e = (2D_m D_{\text{th}})^{1/2}$ (D_e has the dimensions of diffusivity)

Using the data in tables I and II, we find

$$v \ll 40.3 \text{ cm/s} \quad .$$

In that domain, propagation velocity is given by expression (1). We obtain

$$v = \left(\frac{D_{\text{th}}\, P_{jss}}{\Delta H}\right)^{1/2} \quad . \tag{21}$$

At the bottom of Fig. 4, in the area delineated by Eq. (20), v versus I is plotted for the numerical data of Tables I and II; one curve represents the exact solution from Eq. (18) and the other the approximation given by Eq. (21). The two curves are in good agreement, except for values close to the boundary.

IV. Investigation of the High-Velocity Domain

1. Existence of a limit for the induction profile

Given $\eta = v/D_m$, and all other condition being the same, let us consider the effect of a gradual increase in parameter η on the moving induction profile. We find that for a given value of y, if we plot (B/B_0) against the time-dependent variable $s = u/v$, the induction profile becomes distorted until it assumes a limit shape (Fig. 5).

For the data of Tables I and II, the limit profile is reached in plane $y = L_1 + (L_2/2)$ as soon as $\eta > 5000$.

2. Determination of the limit profile

Let us assume that η tends towards infinity in system (14). We have

$$\sum_{k=1}^{+\infty} \frac{a_k^a}{(\alpha_k^2 - \beta_l^2)} = \frac{1}{(1+m)\beta_l^2} \qquad \text{for } l \in N^*$$

It can be shown that, for complex values of z, the meromorphic function defined by

$$H(z) = \frac{\sin z}{z^2\,(\sin z + mz\cos z)} \qquad \text{for } z \in C$$

has poles at zero and at values given by the series $(a_k)_{k\in N}$; it can be expanded[13] into the form

$$H(z) = \frac{1}{(1+m)z} + \sum_{k=1}^{+\infty} \frac{2m}{1+m+(m\,\alpha_k)^2}\,\frac{l}{\alpha_k^2 - z^2} \quad . \tag{22}$$

Writing $z = \beta_l$ in Eq. (22), only the coefficients remain to be identified, hence

$$a_k^a = \frac{2m}{1 + m + (m\alpha_k)^2} \quad .$$

The expression for the limit induction profile in the normal zone is thus

$$B_2^a(y,s) = B_0 \left[1 - \frac{L_3 - y}{(1+m)L_2} + 2\sum_{k=1}^{+\infty} m \frac{\sin[\alpha_k (L_3 - y)/L_2]}{\sin \alpha_k} \frac{\exp(-\alpha_k^2 s/\tau_2)}{1 + m + (m\alpha_k)^2} \right] ,$$

where

$$\tau_2 = \frac{L_2{}^2}{D_m} \qquad (\tau_2 \text{ has the dimension of time}) \ .$$

We have thus reverted to the expression derived in a previous paper[5] for the flux density profile, assuming that the conductor layer, initially in the superconducting state, switches uniformly to the normal resistive state at time $s = 0$.

It can be readily shown that

$$B_2^a(y, s{=}0) = B_0 \qquad \text{for } L_1 \le y \le L_3 \quad .$$

It follows that $B_2^a(y, s)$ is uniform and equal to B_0 in the superconducting zone.

When the flux density profile reaches the limit, the current remains confined in the composite until $s = 0$, at which time it starts diffusing into the superstabilizer as if the entire layer had switched uniformly.

3. Physical interpretation of the limit profile

In the low-velocity domain, the physical interpretation of the limiting case originated from a comparison of the thermal propagation and electromagnetic diffusion phenomena and, more precisely, of the respective ranges of the temperature and magnetic flux density gradients. When demonstrating the existence of a limit profile for flux density, the thermal phenomenon is no longer detected through the temperature profile, but only through the propagation velocity. The physical origin of this new limiting case is thus solely an electromagnetic phenomenon.

Although the flux density profile is dependent on space variables y and z, the dependence relationships are of widely different natures. The electromagnetic diffusion wake develops along (Oy), whereas the shift resulting from thermal propagation occurs along (Oz). Let us assume that the shifting motion is relatively fast compared with the spreading of the electromagnetic wake. At a given time, the transition front can conceivably be located far ahead of the wake itself, i.e., there could be a large distance between the plane $z = vt$ where switching is initiated and the plane where current density has undergone a significant diffusion in the superstabilizer. In the same way, an observer who concentrates on the shifting motion and follows the transition front would hardly notice the electromagnetic diffusion, whereas a second observer monitoring electromagnetic diffusion in plane $z = z_0$, would soon lose sight of the propagation front. Eventually, after switching has been initiated in its plane (at time $t_0 = z_0/v$), the second observer can no longer tell whether the propagation spread was finite or not: he can no longer distinguish it from the change that would have occurred if the entire conductor layer had switched uniformly at time t_0. Our second observer thus ends up equating the flux density profile he sees with the limit profile.

To summarize, the shifting motion of the flux density profile and the spreading of the electromagnetic diffusion wake become decoupled in the high-velocity domain. The electromagnetic phenomenon appears to "forget" the thermal propagation phenomenon from which it originates.

4. Limits of the decoupling range

Our goal now is to determine the values of v for which the flux density profile may be considered as having reached its limit. An ideal way of finding the answer would be to use directly the general expression of $B_2(t,s)$. However, the series (a_k) and (b_k) are not explicitly known, and a purely mathematical criterion could not be found. To resolve this difficulty, we have used the common-sense approach explained below. The validity of that

approach has been verified numerically, so we can therefore be confident that the criterion that we will presently establish is a sufficient condition for the profile to reach its limit.

All other conditions remaining the same, the flux density profile $B_i(y,z-vt)$ undergoes is continuously distorted as v varies. Let us imagine a succession of quasi-stationary states in which the parameter v changes gradually from zero (associated with flux-density profile designated by $B_i^0(y,z)$) to infinity (associated with profile $B_i^a(y,t)$). It can be seen that, for small values of v, the shifting profile will differ little from $B_i^0(y,z-vt)$; for intermediate values, it will be between $B_i^0(y,z-vt)$ and $B_i^a(y,t-z/v)$; for large values of v, it will tend towards $B_i^a(y,t-z/v)$. The attempt to define the decoupling range therefore reduces to establishing a criterion for determining those values of v that make the profile closer to B_i^a than to B_i^0.

Let λ be a length, characteristic of variation of $B_i^0(y,z)$ along (Oz), and τ a time, characterizing the variation of $B_i^a(y,t)$. If the induction profile is close to B_i^0, the length characterizing its variation will be close to λ; on the other hand, if the profile is close to B_i^a, that length will differ little from $v\tau$. Comparing the two characteristic lengths leads to the logical conclusion that the induction profile will approach B_i^a as

$$v \gg \frac{\lambda}{\tau} \quad .$$

Only λ and τ now remain to be determined.

- **Determination of λ:** $B_i^0(y,t)$ is obtained by making $v = 0$ in the general expression derived above for $B_i(y,u)$. In the normal zone, for example, we have

$$B_2^0(y,z) = B_0\left[1 - \frac{L_3-y}{(1+m)L_2} + \sum_{k=1}^{N} m a_k^0 \frac{\sin[\alpha_k(L_3-y)/L_2]}{\sin\alpha_k}\exp\left(-\alpha_k\frac{z}{L_2}\right)\right] \quad ,$$

where the series $(a_k^0)_{k\in[1,N]}$ is found by solving the linear system

$$\sum_{k=1}^{N} \frac{a_k^0}{(\alpha_k-\beta_l)} = \frac{1}{(1+m)\beta_l} \qquad \text{for } 1 \le l \le N \quad .$$

A similar expression can be derived in the case of superconducting zone.

Let us consider a location in the middle of the superstabilizer [in a plane defined by $y = L_1 + (L_2/2)$], and plot the curve $(1/B_0)(\partial B_2^0/\partial z)$ against z (Fig. 6). We will call M_0 the peak of $(1/B_0)(\partial B_2^0/\partial z)$, and we will define λ as the distance between the marks where $(1/B_0)(\partial B_2^0/\partial z)$ equals $M_0/2$.

Thus defined, λ is dependent on m and L_2. Changing to the dimensionless variable $Z = z/L_2$, we now consider $(1/B_0)(\partial B_2^0/\partial Z)$ as a function of Z. We can define a characteristic value Λ, dependent only on m, so that $\lambda = \Lambda L_2$.

Figure 7a shows a plot of Λ against m. It can be seen that $\Lambda \cong 1$ for $m \ll 1$. However, condition (5) for parameter m, which occurs again here, was previously taken as a criterion for superstabilization. It can thus be stated that, in the case of superstabilized conductors $\lambda \cong L_2$.

- **Determination of τ:** the reasoning is the same as for λ, using distance $y = L_1 + (L_2/2)$ and defining τ as the interval between the times when $(1/B_0)(\partial B_2^a/\partial t)$ equals $(M_a/2)$; M_a is the peak value of $(1/B_0)(\partial B_2^a/\partial t)$.

Thus defined, τ depends on m and τ_2. As in the case of Λ, we can change to a dimensionless variable, taking $T = t/\tau_2$, and we can define a characteristic value T, dependent only on m, so that $\tau = T\tau_2$.

Figure 7b shows a plot of T against m. It can be seen that $T \cong 0.1$ for $m \ll 1$ and it can therefore be stated that, in superstabilized conductors, $\tau \cong \tau_2/10$.

NOTE: The factor of ten is due to the fact that the characteristic decay time of $B_i^a(y,t)$ is not τ_2, but τ_2/α_1^2, where the value of α_1 is of the order of π.

To summarize, the decoupling range is delineated, for a given value of parameter m, by

$$v \gg \frac{\Lambda(m)L_2}{T(m)\tau_2} \quad . \tag{23}$$

In the case of superstabilized conductors, Eq. (23) reduces to

$$v \gg 10\frac{L_2}{\tau_2} \quad .$$

Using the data in Tables I and II, we find that

$$v \gg 3.8 \text{ cm/s} \quad .$$

5. An expression for the propagation velocity in the decoupling range

In the decoupling range, Eq. (3) takes the simplified form

$$v\,\Delta H = P_{ja}^*\left(\frac{v}{D_{\text{th}}}\right) \quad ,$$

where P_{ja}^* is the Laplace transformation of the power dissipated along the flux density profile limit.

Since the behavior at the asymptotic limit can be regarded as an instant, uniform transition of the conductor layer, the expression for P_{ja}^* is that computed in Reference 5.

NOTE: In Reference 5, the Laplace transformation was derived with respect to the time variable s; the variable conversion $u = vs$ is therefore required to arrive at the desired expression.

We thus have

$$v = \frac{m\,v_0^2\,L_2/D_e}{\tanh(v\,L_2/D_e) + m\,(v\,L_2/D_e)} \quad , \tag{24}$$

where

$$v_0 = \sqrt{\frac{D_{\text{th}} P_{j0}}{\Delta H}} \quad .$$

(v_0 is the velocity, computed with the assumption that the current remains confined to the composite).

Equation (24) can be put into a dimensionless form by defining the reduced velocity:

$$\nu = \frac{v}{v_0} \tag{25}$$

and the second superstabilization parameter:

$$p = \frac{v_0 L_2}{D_e} \tag{26}$$

We therefore have:

$$\nu = \frac{mp}{\tanh(p\nu) + mp\nu} \tag{27}$$

which shows that v depends only on the two parameters m and p.

The top of Fig. 4, which relates to the domain defined by Eq. (23), shows the curves $v = f(I)$, plotted using the data in Tables I and II; one of the curves represents the exact solution from Eq. (18) and the other the approximation given by Eq. (24). The curves are in perfect agreement.

V. Investigation of Domain Overlap

Figure 4 shows that the decoupling range and the low velocity domain overlap to a certain extent. This is not altogether surprising, since the physical origins of the two limiting cases differ: at low velocities, the temperature profile undergoes an expansion that conceals the electromagnetic diffusion, whereas at high velocities the displacement of the induction profile and the spreading of the electromagnetic diffusion wake become decoupled.

In general, such an overlap occurs when the boundary of the decoupling range, given by (23), is lower than that of the low velocity range, given by Eq. (20), i.e., in cases where

$$\frac{1}{2}\left[\frac{\Lambda(m)}{T(m)}\right]^2 < \frac{D_{\text{th}}}{D_m} \quad , \tag{28}$$

in which the geometrical characteristics of the conductor are only represented by m, the first superstabilization parameter.

For superstabilized conductors, we have determined that the values of (Λ/T) were of the order of 10; Eq. (28) can thus be written $50 < D_{\text{th}}/D_m$. Considering the respective values of D_{th} and D_m, this relationship always holds for superstabilized conductor applications, and the overlap range is relatively wide.

Let us now consider the status of Eq. (24) at low velocities. In this case, we have

$$\frac{v\,L_2}{D_e} \ll 1 \quad .$$

Hence

$$\tanh\left(\frac{v\,L_2}{D_e}\right) \cong \frac{v\,L_2}{D_e} \quad ,$$

and

$$v^2 \cong \frac{m v_0^2}{(1+m)} = \frac{D_{\text{th}} P_{jss}}{\Delta H}$$

which is actually Eq. (21).

Equation (24), which only holds in the decoupling range, is thus an adequate representation of the boundary in the low velocity domain. Since we have shown that the two domains overlap widely, it follows that Eq. (24) applies everywhere.

The above can be summarized by stating that, in superstabilized conductors defined by Eq. (5), the implicit Eq. (18) for propagation velocity can always be reduced to the simplified form of Eq. (24).

VI. Conclusion

A mathematical model has been found for the thermal and electromagnetic behavior of the conductor layer (Fig. 1b) during normal zone propagation; we have thus shown that the temperature and magnetic induction profiles undergo a constant velocity shift, which features an asymptotic limit. In the most general case, propagation velocity is given by Eq. (18) in which the coefficients are determined by linear systems of Eqs. (14) and (15) (N being of the order of 100). For superstabilized conductors defined by Eq. (5), an approximate expression for the propagation velocity is given by Eq. (24), which applies at all points.

Appendix: Evaluation of the Normal Zone Propagation Velocity Along Rectangular Concuctors

This paper considers the plate model of Fig. 1b. A similar study can be conducted for the axi-symmetrical model of Fig. 8. It also yields to a simplified implicit equation for propagation velocity, which in superstabilized conductors applies at all points. This implicit equation can be put into a dimensionless form by defining the two superstabilization parameters,

$$m = \frac{1}{2}\frac{\rho_2}{\rho_1}\frac{L_1^2}{L_3^2 - L_1^2} \qquad \text{and} \qquad p = \frac{v_0 L_{2e}}{D_e} \quad ,$$

where L_{2e} is the equivalent depth of the superstabilizer

$$L_{2e} = \frac{L_3^2 - L_1^2}{2L_1} \qquad \text{(in m)} \quad .$$

This equation then becomes

$$v = \frac{mp}{\dfrac{F_1\left[pv\dfrac{L_3}{L_{2e}} \;\; pv\dfrac{L_1}{L_{2e}}\right]}{G\left[pv\dfrac{L_3}{L_{2e}} \;\; pv\dfrac{L_1}{L_{2e}}\right]} + mpv} \quad , \tag{29}$$

where v is the reduced velocity defined by Eq. (25), and F_1 and G are the functions defined for complex values of z_1 and z_2 by

$$F_1(z_1,z_2) = I_1(z_1)K_1(z_2) - I_1(z_2)K_1(z_1)$$

$$G(z_1,z_2) = I_1(z_1)K_0(z_2) + I_0(z_2)K_1(z_1),$$

and where I_n and K_n are the modified Bessel functions of first and second kind and of order n.

Comparing the definitions of the two superstabilization parameters for the infinite plate and the axi-symetrical models suggest they can be generalized to any geometry under the form

$$m = \frac{\rho_2 A_1}{\rho_1 A_2} \quad \text{and} \quad p = \frac{v_0 L_{2e}}{D_e} \quad ,$$

where

$L_{2e} = A_2/P_d$ is the equivalent depth of the superstabilization (in m);

A_1 and A_2 are the composite and the superstabilizer surfaces (in m^2);

P_d is the composite perimeter in contact with the superstabilizer (in m).

Then a choice has to be made for the propagation velocity equation between Eq. (27) and Eq. (29). Equation (29) would require an equivalent width of conductor L_{3e} to be defined, which would be arbitrary and would have little physical meaning in a rectangular geometry. So, using Eq. (27), the propagation velocity along the conductors of Fig. 1a is given by

$$v = v_{(m,p)} v_0$$

where v_0 is the velocity calculated assuming the current remains confined to the composite, and v is the reduced velocity determined versus m and p.

Figure (9) shows a plot of $v = f(I)$ for the numerical data of Table (III) from the Aleph solenoid.

Acknoledgements

I am grateful to Katharine Metropolis for the considerable help that she provided me while revising the text.

References

[1] Broom, R. F. and E. H. Rhoderick, *Brit. J. of Appl. Phys.*, **11** (1960): 292.

[2] Cherry, W. H. and J. I. Gittleman, *Solid-State Electron.*, **1** (1960): 287.

[3] Desportes, H., J. LeBars, and C. Meuris, "General Design and Conductor Study for the ALEPH Superconducting Solenoid," *J. Phy. (Paris)*–Colloque **45**, (1984): C1–341.

[4] Devred, A. and C. Meuris, in *Proceedings of the 9th International Conference on Magnet Technology*, (Zurich), Sept. 9-13, 1985, eds. C. Marinucci and P. Weymuth (Villegen, Switzerland: SIN, 1985): 577.

[5] Devred, A. "Investigation of Current Redistribution in Superstabilized Superconducting Winding when Switching to the Normal Resistive State," *J. Appl. Phys.* (May 1989, in press).

[6] Hilal, M. A. and R. W. Boom, in *Proceedings of the 9th Symposium on Fusion Technology*, (Garmisch-Partenkirchen, GFR), June 14–18, 1976 (Oxford: Pergamon Press, 1976): 87.

[7] Willig, R. L. "Stability of High-Current Superconductors," *Superconducting MHD Magnet Design Conference*, (Francis Bitter National Magnet Laboratory, MIT), Oct. 18–19, 1978, ed. A. M. Dawson (Cambridge: MIT, 1978):

[8] Scherer, M. and P. Turowski, *Cryogenics*, **15** (1978): 515.

[9] Hirabayashi, H., K. Morimoto, M. Wake, R. Yamada, A. Yamamoto, S. Mori, R. Yoshizaki, H. Kawakami, K. Kondo, K. Aihara, Y. Kazawa, H. Kimura, H. Ogata, R. Saito, S. Suzuki, and Y. Miyake, *Jpn. J. Appl. Phys.*, **20** (1981): 2243.

[10] Devred, A., *Ph. D. diss.*, CEN Saclay (1988), Note CEA–N–2553.

[11] Devred, A., "General Formulas for the Adiabatic Propagation Velocity of the Normal Zone," *IEEE Trans. Magn.* **MAG-25 No. 2,** (1989): 1698.

[12] Goldstein, S., Internal Report SMT/78/25, CEN Saclay (1987).

[13] Lindelöf, E., Le calcul des résidus et ses applications à la théorie des fonctions. (New York: Chelsea Publishing Company, 1947).

Tables

TABLE I ("ALEPH" CONDUCTOR)

Dimensions:

Conductor:		35×3.6 mm^2
Composite:	(Cu/NbTi = 1.35)	4×2 mm^2
Insulation (impregnated glass cloth):		250 μm

Thermal and electrical characteristics (at 7.75 K and 1.5 T):

$C = 5317$ J m^{-3} K^{-1}	$k = 1955$ W m^{-1} K^{-1}	$\Delta H = 10\,730$ J m^{-3}
$\rho_{Cu} = 2.75\ 10^{-10}\ \Omega$m	$\rho_{NbTi} = 5.5\ 10^{-7}\ \Omega$m	$\rho_{Al} = 7.48\ 10^{-11}\ \Omega$m

TABLE II (INFINITE PLATE MODEL)

$L_1 = 1.1$ mm	$L_2 = 16.4$ mm	$L_t = 20.2$ mm

TABLE III (RECTANGULAR MODEL)

$A_1 = 8$ mm^2	$A_2 = 118$ mm^2	$A_t = 165$ mm^2

List of Figures

Figure 1a: Layer of ALEPH conductors.

Figure 1b: Infinite plate model.

Figure 2: Quality of the flux density fit at the boundary between the superconducting and the normal zones. (a) Inside the superstabilizer. (b) Close to the composite.

Figure 3: Convergence of propagation velocity computation.

Figure 4: Exact and approximate solutions for the velocity (infinite plate model).

Figure 5: Plot of the flux density profile showing the existence of an asymptotic limit for large velocities.

Figure 6: Characteristic length of variations of a flux density profile shifting infinitely slowly.

Figure 7: Parameters used for delimiting the high-velocity domain. (a) For a flux density profile shifting infinitely slowly. (b) For a flux density profile shifting infinitely fast.

Figure 8: Axi-symmetrical model.

Figure 9: $v = f(I)$ curves (ALEPH conductor).

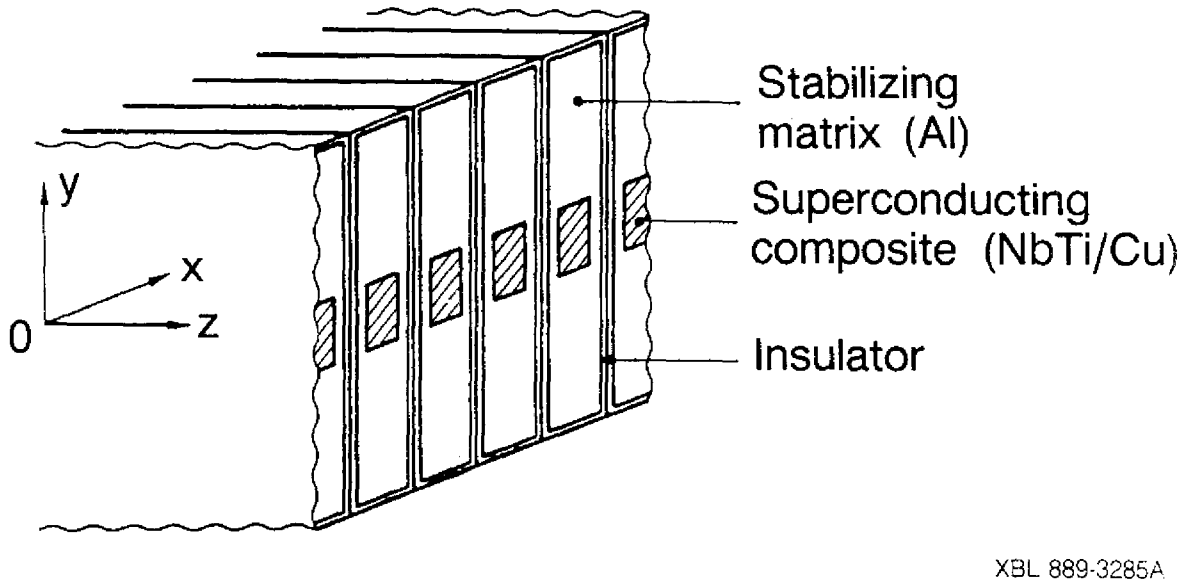

Figure 1a: Layer of ALEPH conductors.

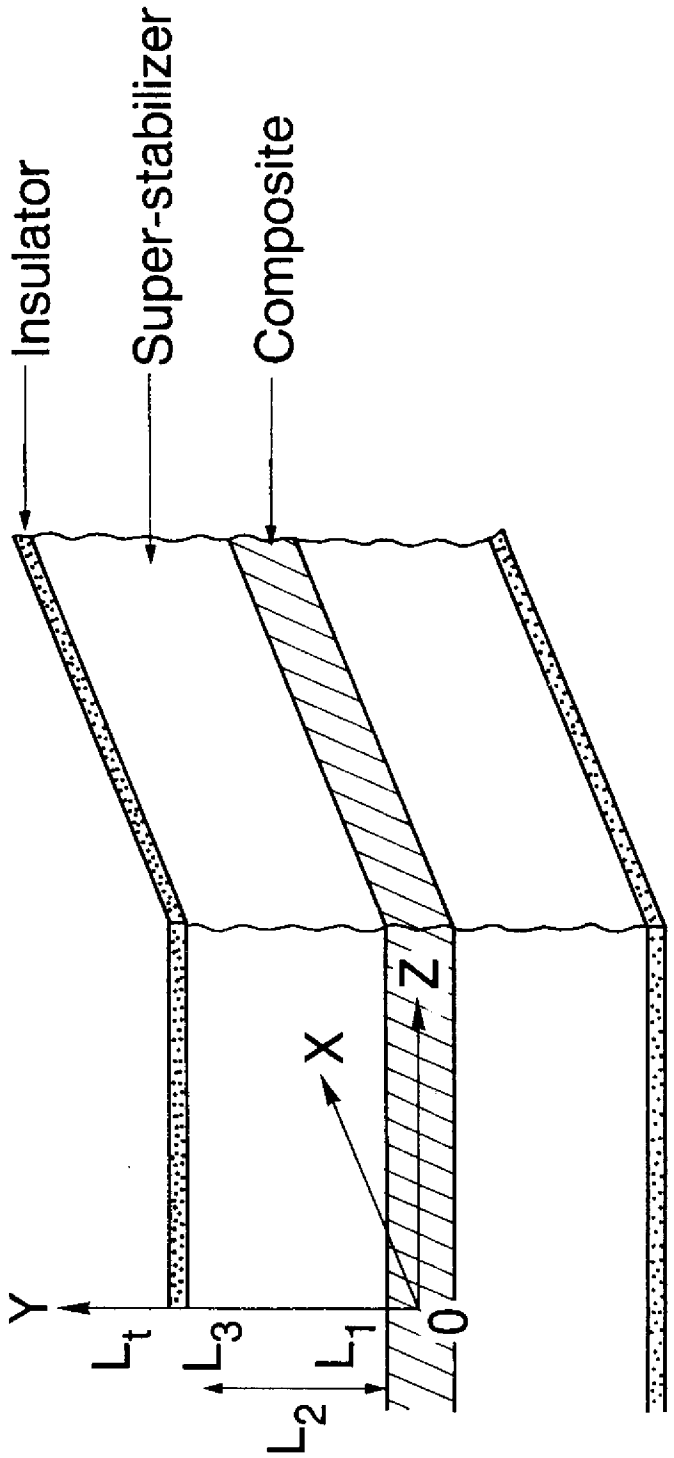

XBL 891-7026

Figure 1b: Infinite plate model.

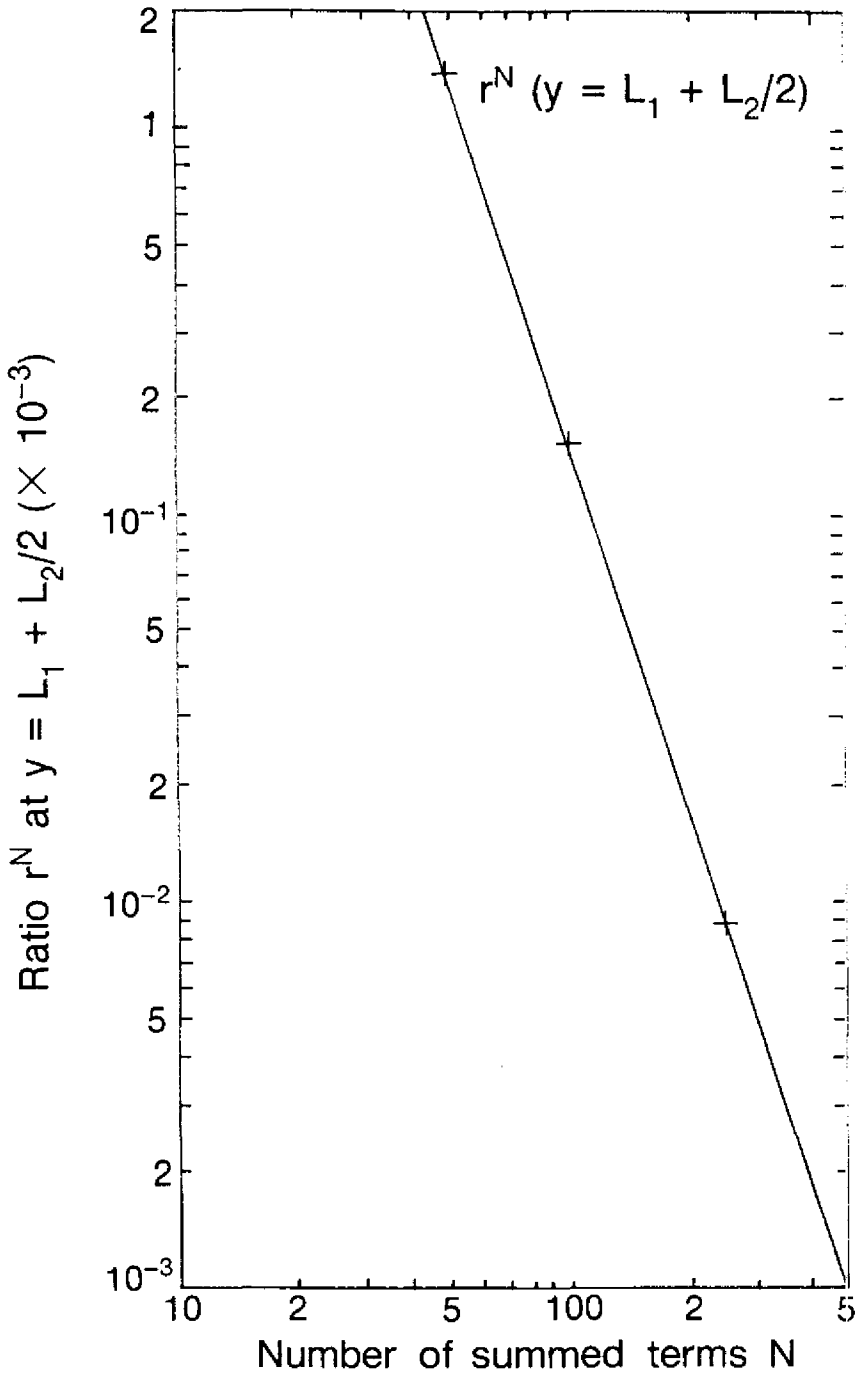

XBL 891-7027

Figure 2a: Quality of the flux density fit at the boundary between the superconducting and the normal zones, inside the superstabilizer.

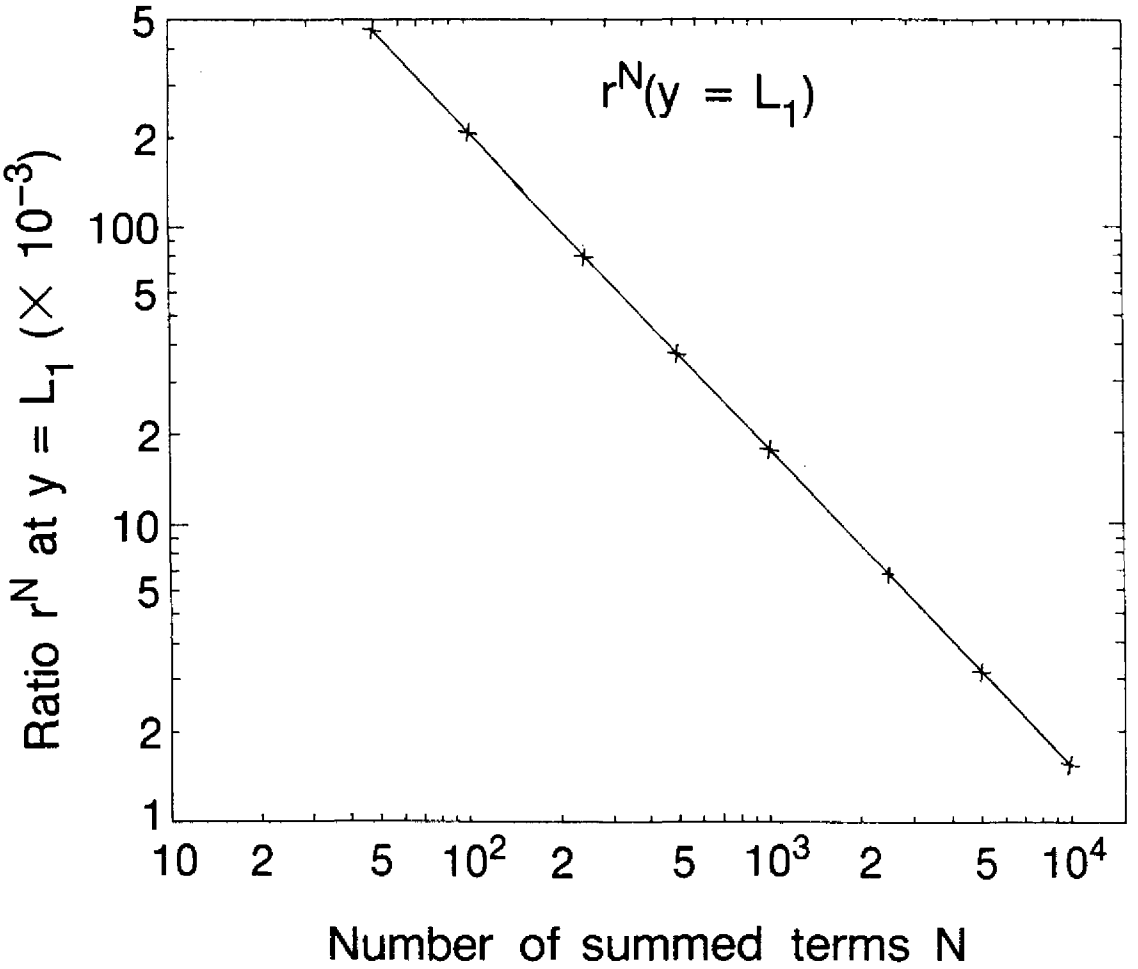

XBL 891-7028

Figure 2b: Quality of the flux density fit at the boundary between the superconducting and the normal zones, close to the composite.

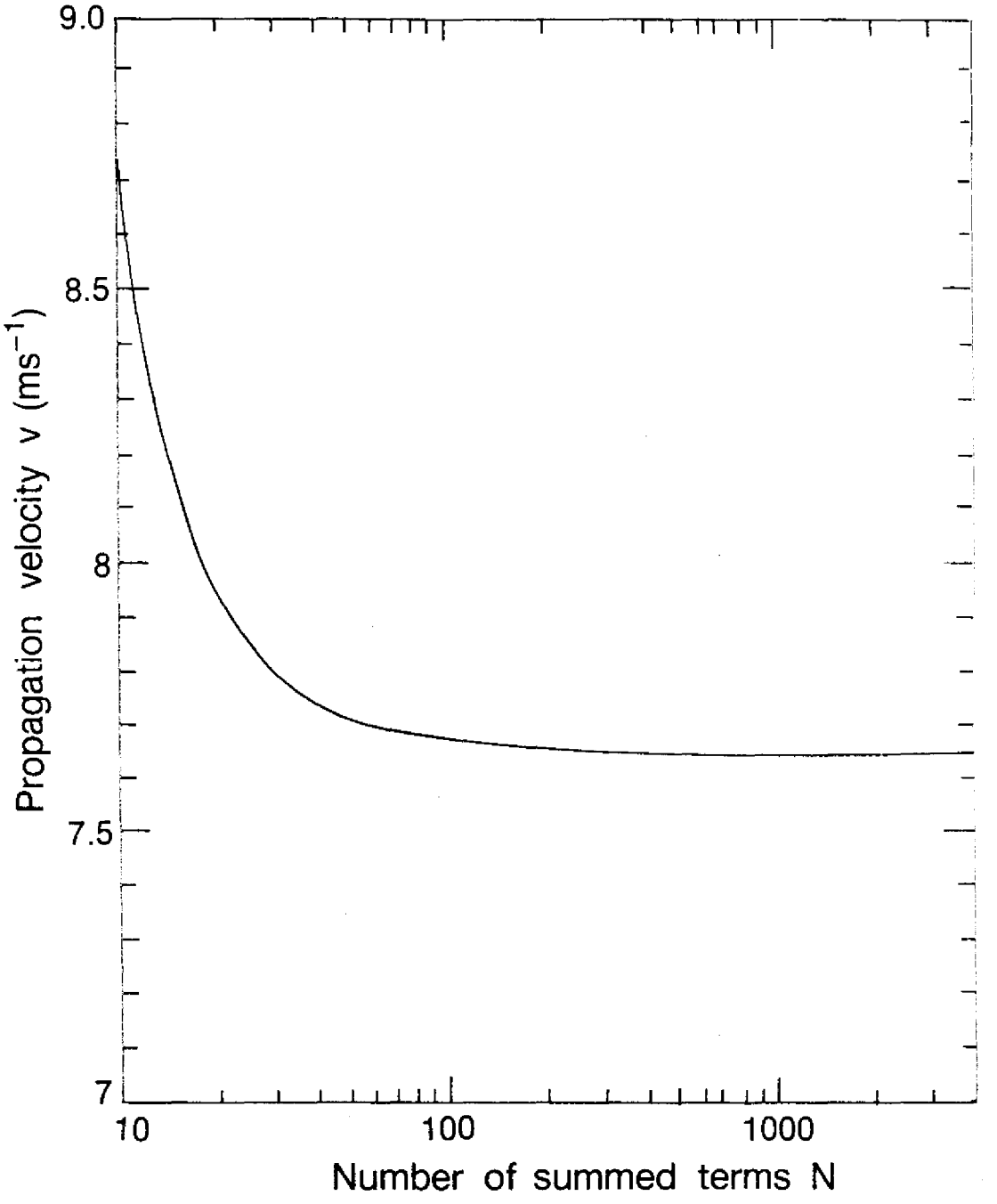

XBL 891-7029

Figure 3: Convergence of propagation velocity computation.

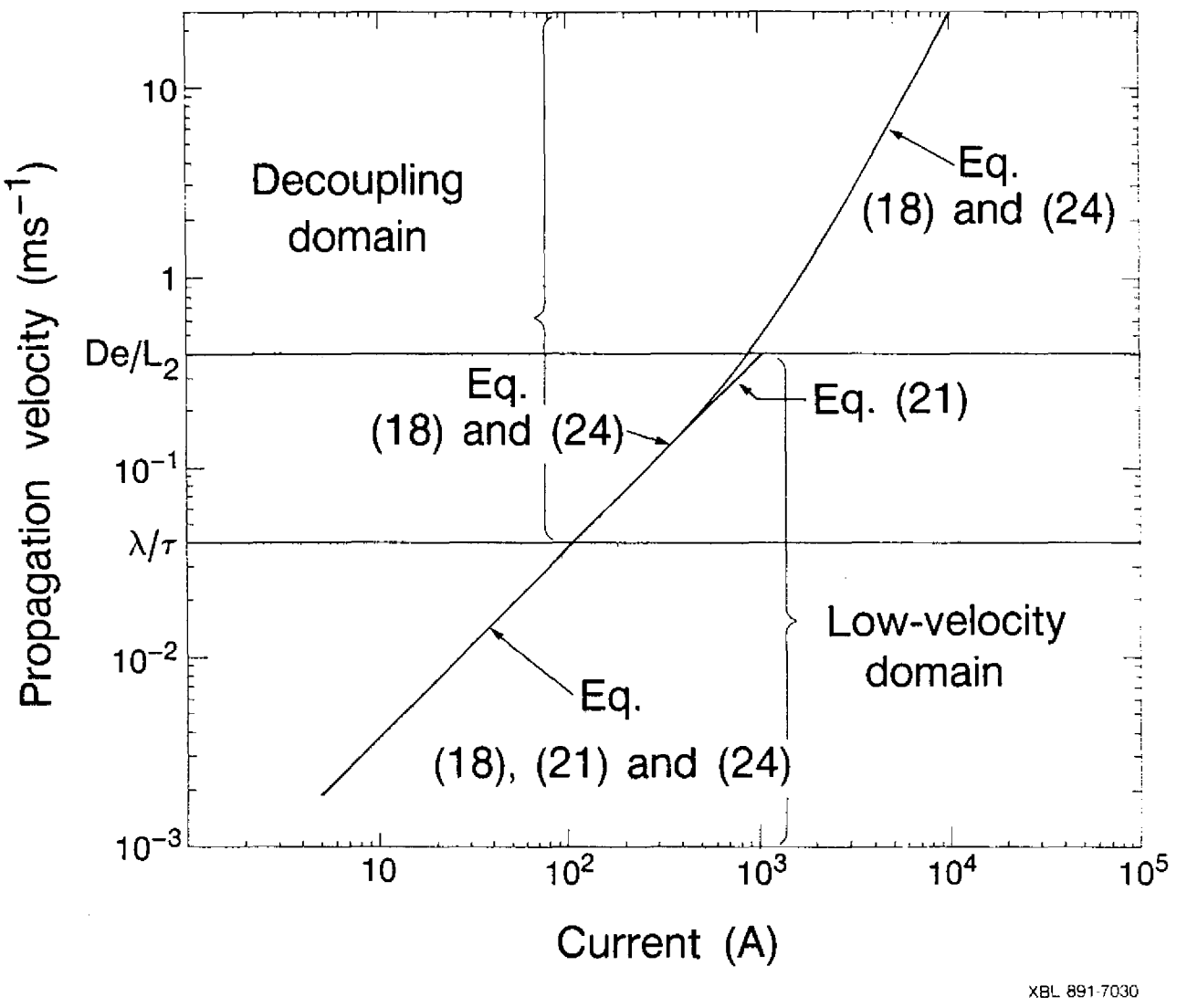

Figure 4: Exact and approximate solutions for the velocity (infinite plate model).

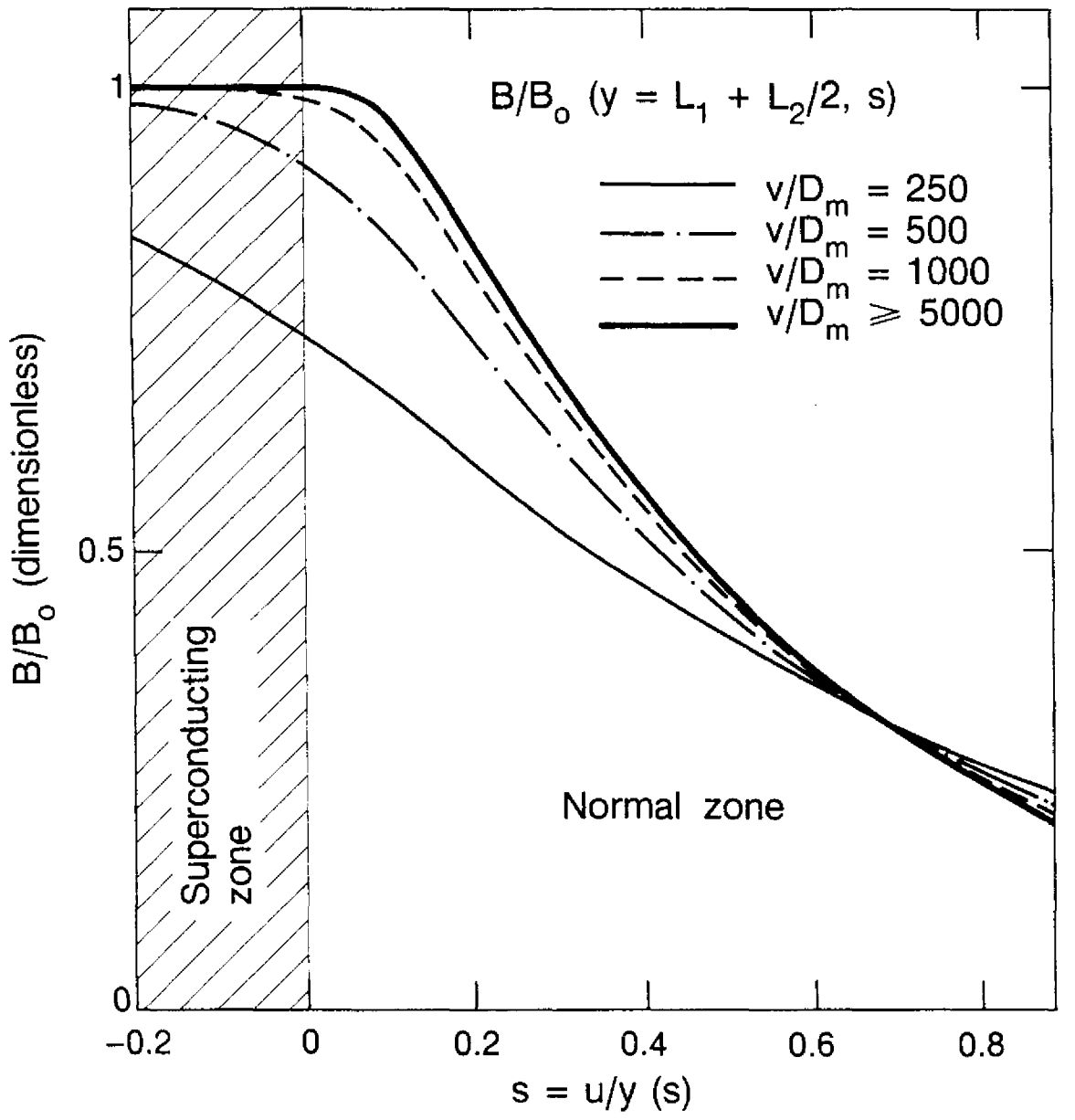

XBL 891-7035

Figure 5: Plot of the flux density profile showing the existence of an asymptotic limit for large velocities.

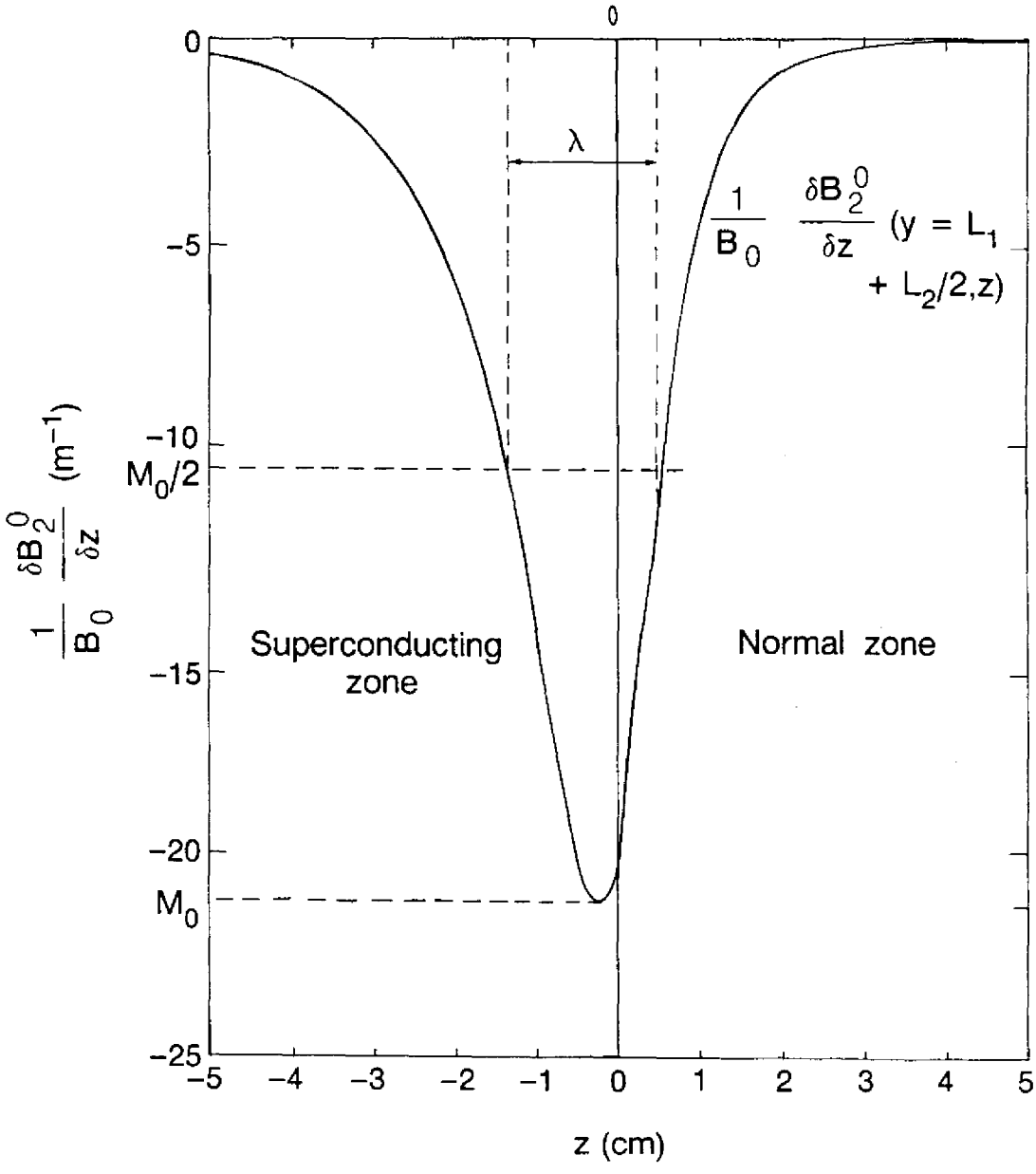

Figure 6: Characteristic length of variations of a flux density profile shifting infinitelely slowly.

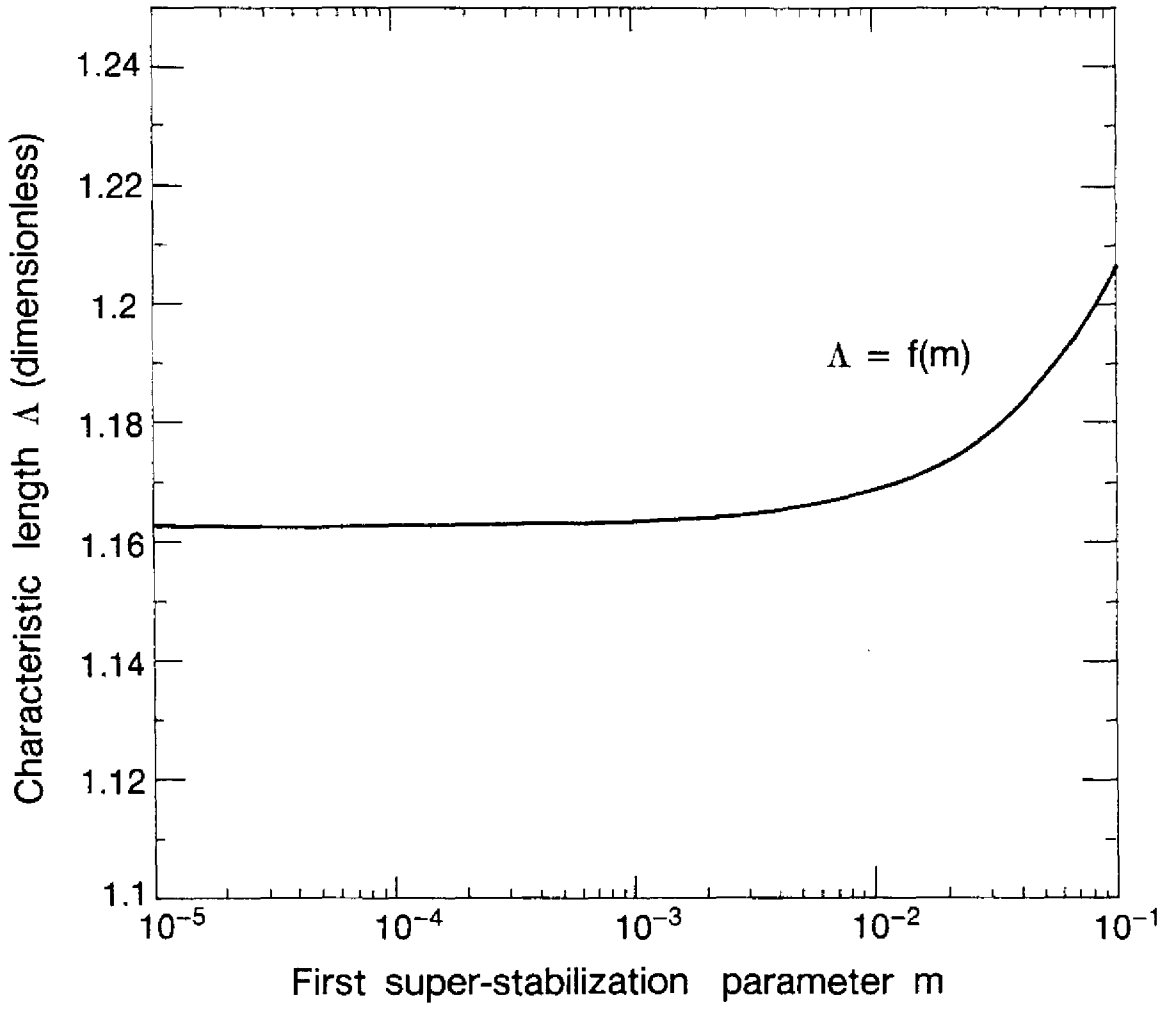

XBL 891-7031

Figure 7a: Characteristic parameter of a flux density profile shifting infinitely slowly.

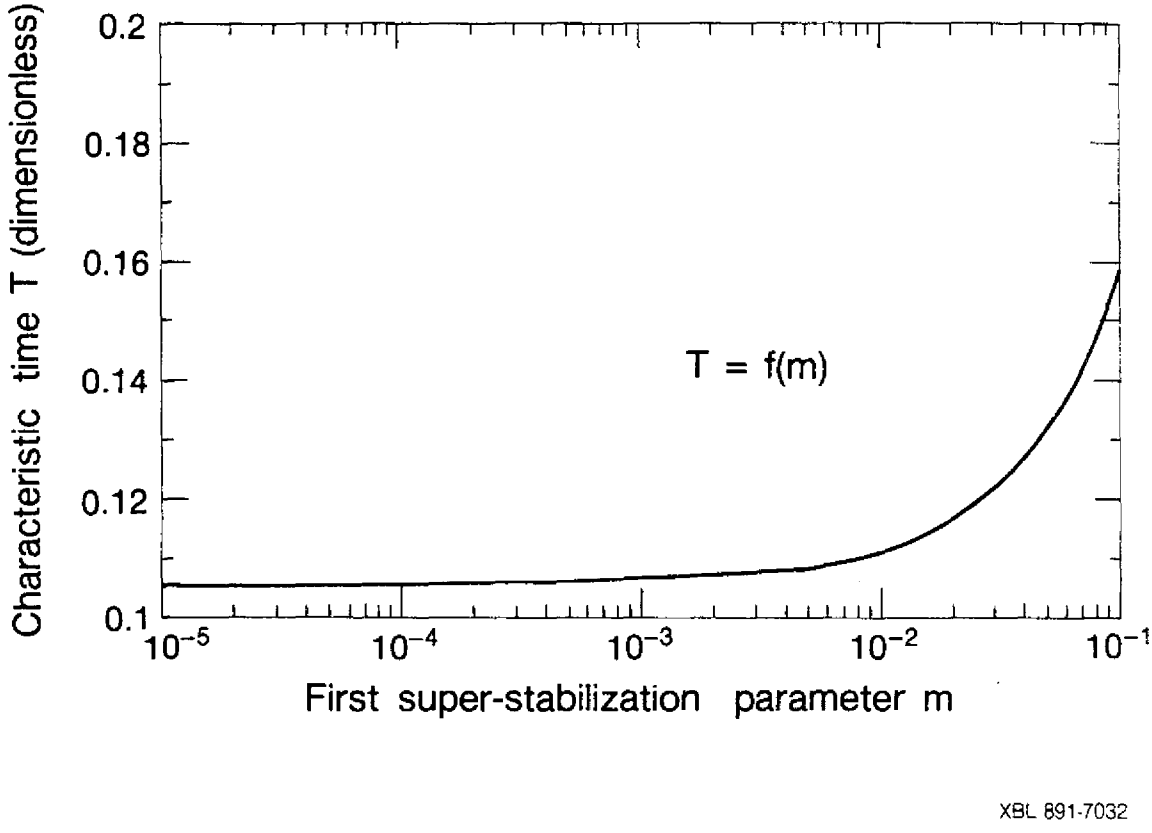

Figure 7b: Characteristic parameter of a flux density profile shifting infinitely fast.

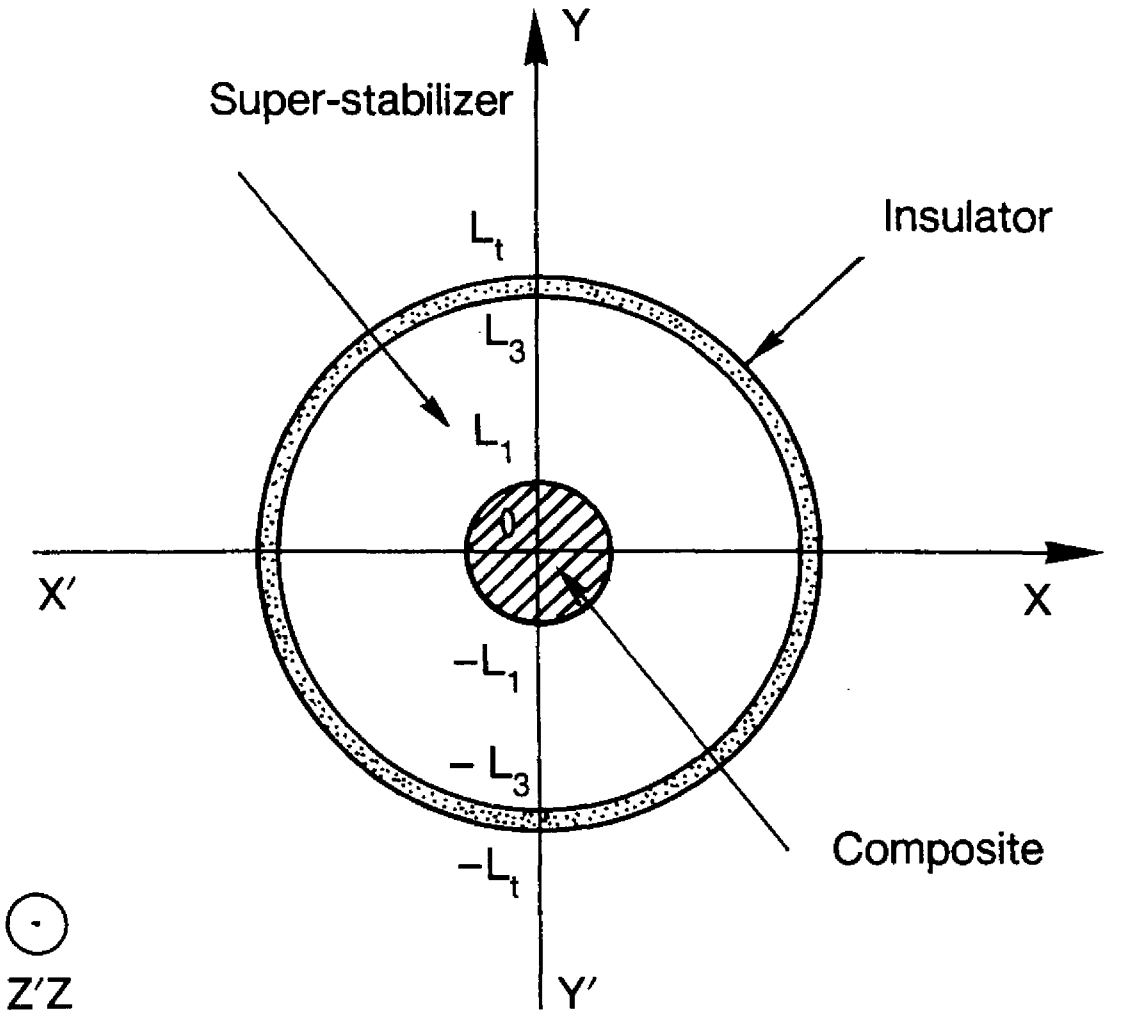

XBL 891-7033

Figure 8: Axy-symmetrical model.

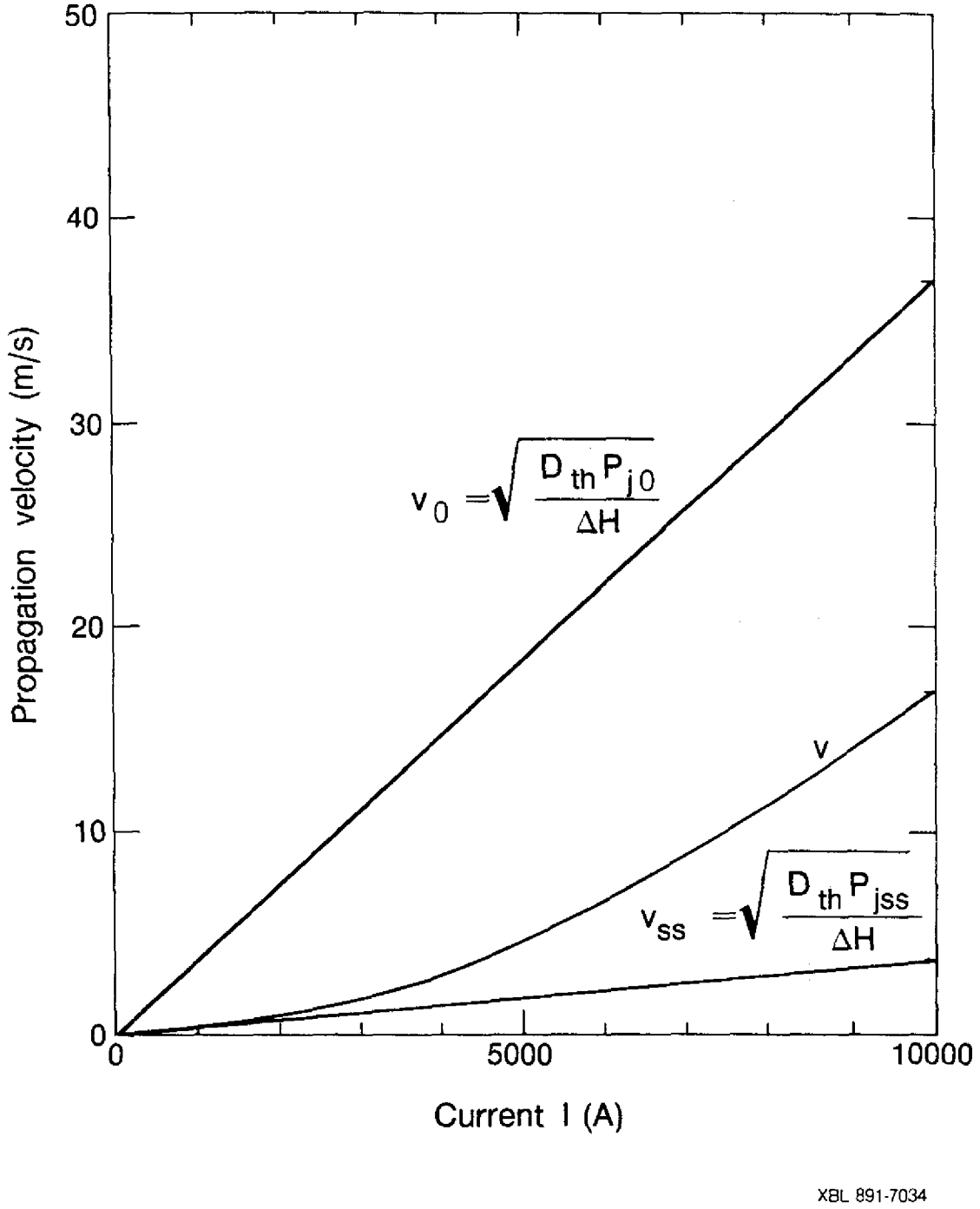

Figure 9: $v = f(I)$ curves (ALEPH conductor).